

This work was written as part of one of the author's official duties as an Employee of the United States Government and is therefore a work of the United States Government. In accordance with 17 U.S.C. 105, no copyright protection is available for such works under U.S. Law.

Public Domain Mark 1.0

<https://creativecommons.org/publicdomain/mark/1.0/>

Access to this work was provided by the University of Maryland, Baltimore County (UMBC) ScholarWorks@UMBC digital repository on the Maryland Shared Open Access (MD-SOAR) platform.

Please provide feedback

Please support the ScholarWorks@UMBC repository by emailing scholarworks-group@umbc.edu and telling us what having access to this work means to you and why it's important to you. Thank you.



ATMOSPHERIC SCIENCE

Observational evidence of strong forcing from aerosol effect on low cloud coverage

Tianle Yuan^{1,2*}, Hua Song^{2,3}, Robert Wood⁴, Lazaros Oreopoulos², Steven Platnick²,
Chenxi Wang^{1,2}, Hongbin Yu², Kerry Meyer², Eric Wilcox⁵

Aerosols cool Earth's climate indirectly by increasing low cloud brightness and their coverage (Cf), constituting the aerosol indirect forcing (AIF). The forcing partially offsets the greenhouse warming and positively correlates with the climate sensitivity. However, it remains highly uncertain. Here, we show direct observational evidence for strong forcing from Cf adjustment to increased aerosols and weak forcing from cloud liquid water path adjustment. We estimate that the Cf adjustment drives between 52% and 300% of additional forcing to the Twomey effect over the ocean and a total AIF of $-1.1 \pm 0.8 \text{ W m}^{-2}$. The Cf adjustment follows a power law as a function of background cloud droplet number concentration, N_d . It thus depends on time and location and is stronger when N_d is low. Cf only increases substantially when background clouds start to drizzle, suggesting a role for aerosol-precipitation interactions. Our findings highlight the Cf adjustment as the key process for reducing the uncertainty of AIF and thus future climate projections.

INTRODUCTION

Tiny airborne particles—aerosols—can affect the energy balance of Earth's climate by modifying cloud brightness and coverage (1, 2). The resulting energy balance perturbation constitutes a radiative forcing, known as the aerosol indirect forcing. It partially offsets the positive forcing due to greenhouse gases. Given the observed global temperature increase and positive forcing from greenhouse gases, strong negative aerosol indirect forcing implies a high climate sensitivity because the observed warming would have been a result of a small net positive forcing (3). The total aerosol indirect forcing is estimated to be between -1.7 and -0.3 W m^{-2} based on observations and represents the largest source of uncertainty in our forcing estimates (3). The uncertainty range— 1.4 W m^{-2} —is about half of the historic forcing from greenhouse gases and leads to considerable uncertainty in climate sensitivity estimated using historic data, which has important implications for climate adaptation and mitigation plans (4).

Marine low clouds are the largest contributor to reflecting solar radiation back to space and aerosol effects on them contribute substantially to the total aerosol indirect forcing. The fraction of reflected solar radiation is largely determined by three cloud parameters of marine low clouds: liquid water path (LWP), cloud droplet number concentration (N_d), and cloud coverage (Cf). Aerosols can modify all three through changing N_d . Increasing aerosol concentration leads to higher N_d and smaller cloud droplet effective size (R_e), which makes marine low clouds brighter if LWP and Cf remain constant, the so-called Twomey effect (1). The Twomey effect is widely supported by observational evidence. However, LWP and Cf do adjust to changes in N_d and R_e . The decreased R_e from increasing N_d can delay and suppress precipitation formation by suppressing the droplet collision-coalescence process. Suppressed

precipitation in turn can increase LWP and Cf by reducing the cloud water sink and help clouds to live longer (2). However, other physical processes can work against this chain reaction (5, 6). For example, smaller and more numerous droplets can introduce stronger evaporation when mixed with dry environmental air, thus increasing the cloud water sink to the ambient air and decreasing LWP and Cf (5). Such processes form complex feedback loops in the cloud system that give rise to the final LWP and Cf adjustments. A key unknown is how much additional forcing is introduced by these adjustments in addition to the Twomey effect.

Global satellite observations can provide empirical estimates on these adjustments (3, 7). There is growing evidence that the LWP adjustment can be bidirectional and depends on the background conditions (8–10). Existing evidence for Cf adjustment is more limited and less well-quantified, which manifests in a wide uncertainty range in the forcing due to Cf adjustment (3, 7), despite clear evidence of Cf increase in response to ship-emitted aerosols in case studies (11, 12). Some studies use correlation and covariance between satellite observed LWP and Cf and aerosol loading, but their results can be affected by retrieval biases of aerosols and clouds, aerosol swelling with humidity, unresolved vertical profiles of aerosols and clouds (13), and removal by precipitation, among other possible confounding correlations (3). Other studies instead analyze the covariance using derived N_d , instead of aerosol loading, to alleviate aerosol retrieval bias complications and still find contrasting responses of LWP to N_d and increasing Cf to N_d (14–16). However, retrieval artifacts and potential confounding correlations still exist. For example, derived N_d is biased low for broken and low-Cf clouds and the positive correlation between N_d and Cf can at least partially be attributed to this bias (3, 17). Such relationships remain correlational and do not constitute causality, which introduces uncertainty in attributing and quantifying the forcing due to the LWP and Cf adjustments.

Here, we directly measure the cloud LWP and Cf adjustments attributable to aerosol influences by contrasting polluted clouds in ship-tracks with nearby background clouds, overcoming the limitation of correlation studies. Our main goal is to quantify the ratio

¹Goddard Earth Sciences Technology and Research (GESTAR) II, University of Maryland, Baltimore County, Baltimore, MD, USA. ²Sciences and Exploration Directorate, Goddard Space Flight Center, Greenbelt, MD, USA. ³SSAI Inc., Lanham, MD, USA. ⁴Department of Atmospheric Sciences, University of Washington, Seattle, WA, USA. ⁵Desert Research Institute, Reno, NV, USA.

*Corresponding author. Email: tianle.yuan@nasa.gov

of contributions of the LWP and Cf adjustments to the total aerosol indirect forcing compared to that of the Twomey effect [e.g., (10)]. We use ship-tracks as our “opportunistic experiments” (10, 18), where the LWP and Cf adjustments can be attributed to ship-emitted aerosols, to avoid the covariance between LWP and Cf and N_d that are driven by meteorology and other confounding factors (18) (Fig. 1). Previous analyses of ship-tracks and similar opportunistic experiments suggest variable LWP adjustments to aerosols (10, 19–21). Toll *et al.* (10) show a slight LWP increase in ship-tracks on average and the magnitude partially results from the balance between entrainment drying and moistening by precipitation suppression. The Cf adjustment, though clearly observed and modeled (22–24) in case studies, has not been systematically quantified using ship-track observations and remains highly uncertain (3, 7). We assemble a large collection of ship-track samples and analyze the LWP and Cf adjustments with them to address the knowledge gap.

RESULTS

Ship-track sampling and mean cloud response

We previously developed an algorithm to automatically detect ship-tracks globally in the Aqua Moderate Resolution Imaging Spectrometer (MODIS) data and produce ship-track masks that include pixels polluted by ship-emitted aerosols (25, 26) (Fig. 1 and figs. S1 and S2 in Materials and Methods). Here, we use ship-tracks derived from the algorithm. A separate analysis algorithm

finds surrounding background cloud pixels with a width of 20 MODIS pixels, equivalent to around 20 km (see Materials and Methods). We contrast the properties of polluted and background low clouds using MODIS retrievals within individual 128 pixel \times 128 pixel blocks (see Materials and Methods for details). We choose the size of 128 pixels \times 128 pixels to have sufficient pixel counts in a block to obtain accurate estimate of cloud fractions in both ship-track and control clouds. In total, we find 295,036 blocks with ship-tracks in 18 years of Aqua MODIS record (Fig. 2 and Materials and Methods). Our total number of ship-track pixels is equivalent to around 12 million ship-track segments as defined in Toll *et al.* (10) assuming an average ship-track width of 10 pixels, representing an increase of several orders of magnitudes in the number of samples. Our samples include ship-tracks of many different sizes and thus ages.

The ship-track samples cover wide range of meteorology and background cloud conditions over the global ocean (fig. S3). Nearly all ship-tracks occur in a relatively stable environment with the estimated inversion strength (EIS) (27) greater than 0 K. The cloud top height of our samples has a wide range between a few hundred meters and a couple of kilometers with a peak at around 800 m. The above cloud top relative humidity (RH) ranges between 10 and 90%, and its distribution has two local maxima at 10 and 90%. Background N_d ranges from a few droplets cm^{-3} to a few hundred droplets cm^{-3} with a strong peak at the low end. We include most ship-track samples in our analysis, recognizing that ship-track detectability has a wide range (23) and implicit

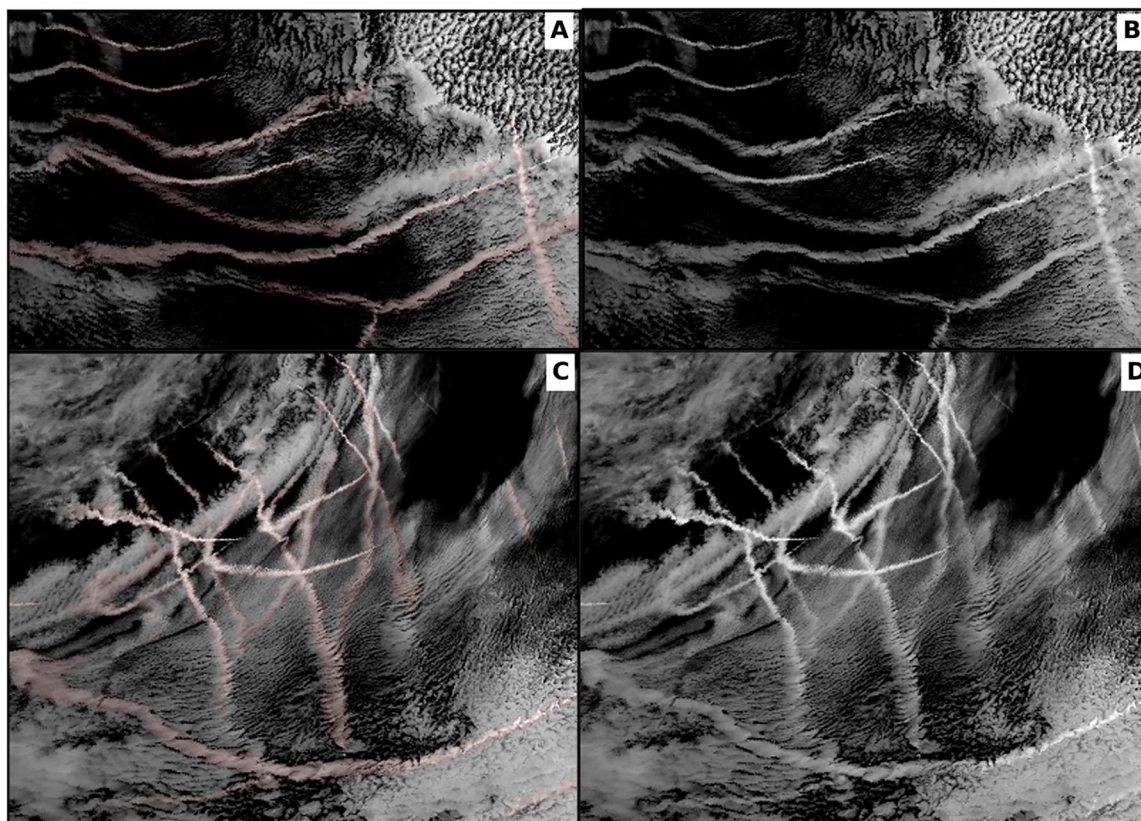


Fig. 1. Example images of ship-tracks and detected ship-track masks. MODIS Aqua images of 2.1- μm reflectance overlaid with detected ship-track mask in pink (A) and true color (B) at 21:25 UTC, 29 June 2005, and the same at 22:25 UTC, 12 July 2010 (C and D).

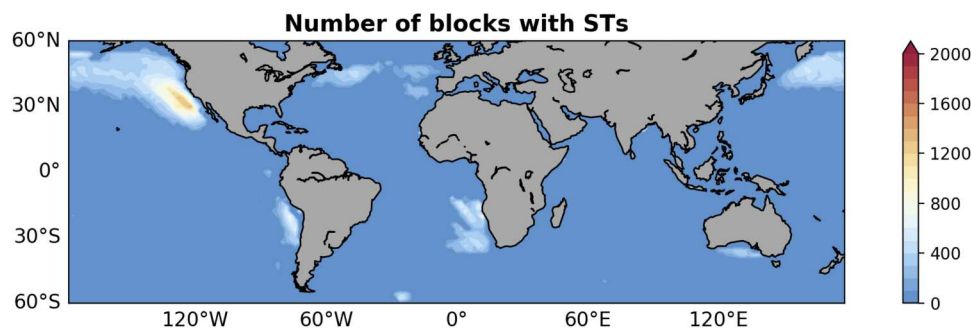


Fig. 2. Frequency of ship-track containing blocks. The Northern Pacific has the most samples. Considerable number of samples also come from the southeast Pacific, the southeast Atlantic, the northern Atlantic, and to the south of Australia.

sampling bias can be introduced by imposing filters (see discussion in Materials and Methods and figs. S4 and S5). Notable changes in probability distribution functions (PDFs) of background cloud properties occur when samples are filtered using different criteria (fig. S4). On average, we measure a reduction of $2.9 \mu\text{m}$ in R_e and increases of 5.8 g/m^2 and 9% in LWP and Cf in polluted clouds within ship-tracks compared to the background clouds (Fig. 3). The SDs of such changes are $2 \mu\text{m}$, 44 g/m^2 , and 19%, respectively. They are much larger than the mean change for the LWP and Cf, highlighting strong variability in the adjustments of these variables.

Cf and LWP adjustments and the role of background conditions

The Cf adjustment to additional aerosols is a positive and nonlinear function of background N_d or R_e (Fig. 4). The mean absolute Cf increase in all ship-track samples is 9%. We note that the mean value is a simple average and does not account for occurrence frequency of background cloud conditions, which is addressed when we later calculate radiative effect from Cf adjustment. Our method allows for bidirectional Cf adjustments, but only in a small percentage of cases is Cf adjustment negative (Fig. 3). Small average Cf increases (1 to 2%) are observed in clouds where mean R_e is smaller than $14 \mu\text{m}$, or mean N_d greater than 60 cm^{-3} . Once background clouds are cleaner than the threshold, i.e., N_d less than 60 cm^{-3} or mean R_e greater than around $14 \mu\text{m}$, the sensitivity of Cf to N_d , dCf/dN_d , increases

substantially with decreasing background N_d , or increasing R_e . Our results agree with similar N_d threshold behavior previously reported using different approaches and data (21). The $14\text{-}\mu\text{m}$ threshold is physically meaningful because low clouds start to produce substantial drizzle that depletes cloud water once R_e exceeds the $14\text{-}\mu\text{m}$ threshold (28). Further increase in R_e and thus precipitation rate can quickly deplete cloud water and reduce Cf. Our measurements indicate that the Cf increase due to aerosols only becomes substantial under such background cloud conditions, likely through precipitation suppression, which supports the conceptual mechanism proposed by Albrecht (2).

Moreover, Cf increase due to aerosols is a super-linear function of R_e or N_d and proportional to $e^{0.29 \times R_e}$ or $N_d^{-1.5}$, indicating that the rate of Cf increase accelerates with cleaner background clouds with larger R_e . Quantitatively, the measured rate of Cf increase is at a rate of 1.2% per 1 cm^{-3} when the background N_d is at 9 cm^{-3} , which is very close to the simulated value of 1.4% per 1 cm^{-3} at the same background N_d in Possner *et al.* (23) using a large-eddy simulation model with detailed physics. At a background N_d of 20 cm^{-3} , the rate decreases to 0.45% per 1 cm^{-3} . The tight exponential fit, $dCf/dN_d \propto e^{0.29 \times R_e} \mid R_e > 14 \mu\text{m}$, suggests that addition of aerosols can reverse the runaway depletion of cloud water and decrease of Cf by precipitation. Addition of aerosols in an aerosol-limited regime can strongly increase Cf, which qualitatively supports observations and modeling results of ship-emitted aerosols reversing low Cf scenes to

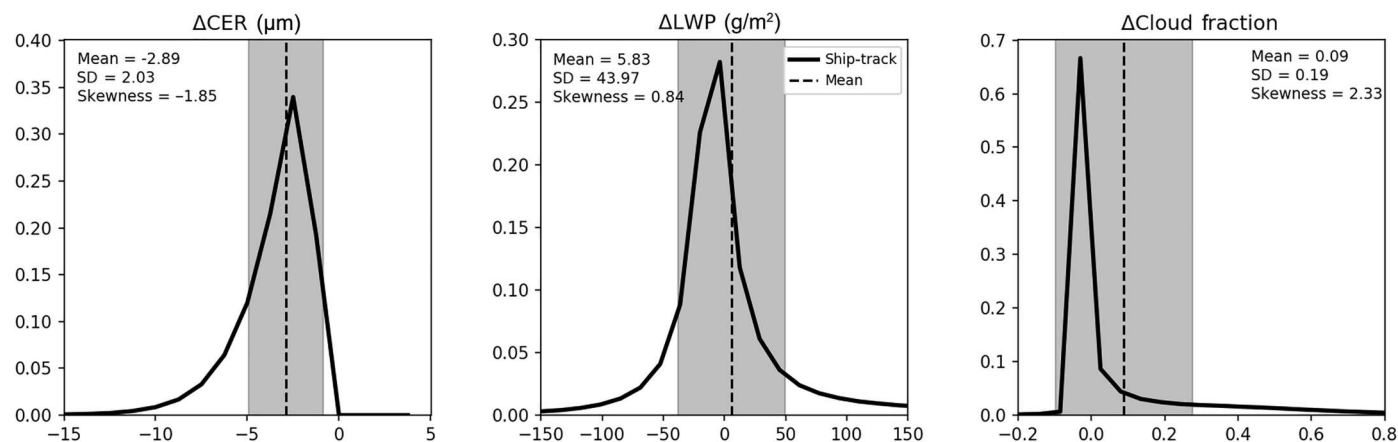


Fig. 3. Distributions of bulk cloud adjustments. PDFs of ΔR_e , ΔLWP , and ΔCf for individual $128 \text{ pixel} \times 128 \text{ pixel}$ MODIS blocks that contain ship-tracks (see Materials and Methods). The mean values are indicated by the dashed vertical lines and the ± 1 SD range is in gray shading.

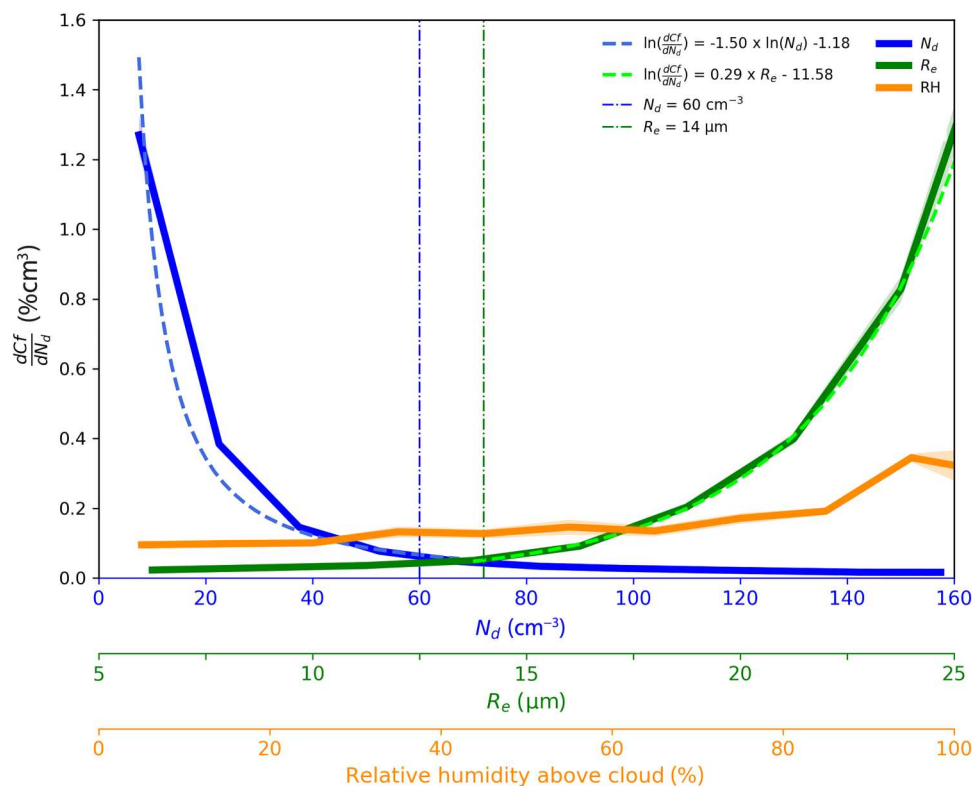


Fig. 4. Dependence of coverage adjustment on background conditions. dCf/dN_d for each bin of the background cloud N_d , R_e , and RH above the cloud, where Cf represents low cloud fraction. The blue and green dashed lines are functional fit to the data. The vertical dashed lines are for constant N_d and R_e at 60 cm^{-3} and $14 \text{ }\mu\text{m}$, respectively. Each solid, colored line has an x axis with the same color and associated uncertainty range is plotted as shades around the solid line. The range represents the 5 to 95% range.

nearly overcast ones (11, 12, 22, 23). Our analyses show that the effects of aerosol-cloud-precipitation interactions on Cf are nonlinear and depend on background conditions (29, 30). This measurement-based relationship provides valuable quantitative constraints on the Cf adjustments to aerosols under different background conditions.

The Cf adjustment also has clear dependence on the background Cf . On average, dCf/dN_d is negatively correlated with the background Cf . The sensitivity is at zero when background Cf is around 1 and peaks at about 3% per 1 cm^{-3} when the background Cf is about 0.2. Cf of 0.2 is notably lower than the mean Cf for open cellular clouds, at around 0.5 (31), and close to that of marine low clouds with heavy drizzle (32). The combination of low Cf and heavy drizzle points to an aerosol-limited cloud regime primed for high dCf/dN_d , which agrees with the relationship between dCf/dN_d and R_e and observations of ship-tracks appearing overcast within a low Cf and precipitating environment (12, 18, 20) (e.g., Fig. 1).

The average LWP adjustment, \overline{dLWP} , is 5.83 gm^{-2} with a large SD of 31 gm^{-2} . The fairly small \overline{dLWP} results from substantial dLWP in both positive and negative directions in individual ship-track samples, reaffirming results from previous studies (10, 19–21, 33). Forty-eight percent of the ship-track samples have negative dLWP although \overline{dLWP} is close to zero and positive. The relative sensitivity of LWP to N_d , $d\ln LWP/d\ln N_d$, is found to be a function of the background N_d (or R_e) and above cloud RH (10, 24). $d\ln LWP/$

$d\ln N_d$ starts to be positive when above cloud RH is greater than 85%, and N_d is less than 45 cm^{-3} (Fig. 5). The dependence of LWP adjustment on above cloud RH supports the idea that the balance between the effects of entrainment drying and moistening by precipitation suppression (5, 10) partially determines the LWP adjustment. Its N_d dependence may reflect the aerosol effect on precipitation. The 45 cm^{-3} threshold suggests that once appreciable precipitation develops, aerosols tend to suppress the cloud water depletion by precipitation and increase LWP and Cf . When precipitation is not strong enough, the effect of drizzle suppression by aerosols on LWP can be counterbalanced by increased entrainment drying if the above cloud RH is low (34). However, more factors may be at play in the LWP adjustment than just the balance between precipitation suppression and entrainment drying such as cloud top height, boundary stability, and sea surface temperature (SST) (10).

Unlike LWP, the sensitivity of Cf to aerosols has weak dependence on the above cloud RH (Fig. 4). The mean dCf/dN_d is around 0.1% per cm^{-3} when averaged under most RH values, and its uncertainty range relative to the mean is considerably larger than that using background N_d or R_e as the explanatory variable. This suggests that above cloud RH plays a minor role in determining Cf adjustment and supports the primary role of aerosol-cloud-precipitation interactions in driving Cf adjustment.

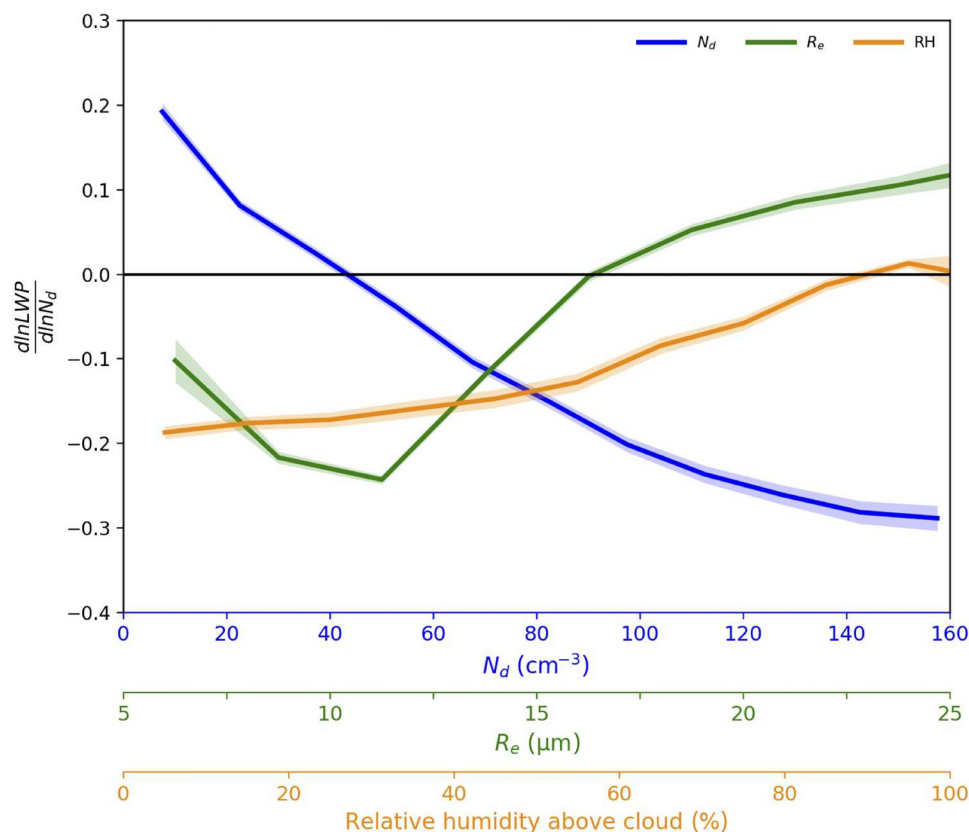


Fig. 5. Dependence of LWP adjustment on background conditions. The dependence of $d\ln LWP/d\ln N_d$ on above cloud top relative humidity, background R_e , and N_d . Plot setup is similar to Fig. 4.

Forcing due to Cf and LWP adjustments

Our analysis shows that aerosols in ship-tracks make clouds brighter mainly through the Twomey effect with a minor contribution from the LWP adjustment because $dLWP$ is only 5.83 g/m^2 . However, the range of LWP adjustments is wide and depends on background meteorology and cloud conditions, leading to a range of possible responses, from strong cancelation of the Twomey effect due to LWP reduction to strong enhancement by LWP increases. Ship-emitted aerosols also make the whole scene brighter by increasing Cf in addition to increasing existing clouds' brightness. The Cf adjustment is substantial (e.g., Fig. 3) because an absolute increase of 3.5 to 5% in low Cf would be enough to counterbalance the positive forcing of CO_2 doubling (35, 36), which suggests that the Cf adjustment at local regions can be substantial. The Cf adjustment also depends sensitively on the background R_e or N_d , and Cf.

We quantify the relative contribution of the LWP and Cf adjustments to the total aerosol indirect forcing to that of the Twomey effect over the global ocean. We apply the dependence of the dCf/dN_d and $d\ln LWP/d\ln N_d$ on the background N_d as measured in ship-tracks to global observations. The N_d change is produced by global chemical transport model simulations (10). We also consider the effects of cloud albedo, low cloud fraction, cloud overlap between high and low clouds, Cf change, and solar flux (see Materials and Methods for details). Our calculations show that the LWP adjustment effect is only adding 1% of radiative cooling to the Twomey effect when averaged over global oceans. The estimated forcing from the Twomey effect is -0.75 W m^{-2} , which is close to the consensus

(3). The forcing from the LWP adjustment represents an additional contribution of 1% on top of the Twomey effect, and is estimated to be $-0.0083 \pm 0.012 \text{ W m}^{-2}$ (Fig. 6 and table S1).

The effect of Cf adjustment, however, contributes an additional 52% cooling relative to the Twomey effect. The estimated radiative forcing from the Cf adjustment is $-0.39 \pm 0.01 \text{ W m}^{-2}$. Our estimate would suggest the total aerosol indirect forcing to be $-1.1 \pm 0.8 \text{ W m}^{-2}$ given the current best estimate of the Twomey effect is $-0.7 \pm 0.5 \text{ W m}^{-2}$ (3, 7). The absolute magnitudes of the forcing due to the two adjustments are subject to retrieval uncertainties in cloud variables and the estimated ΔN_d as discussed in detail in Materials and Methods. Their relative contributions to the Twomey effect, however, are less sensitive to such uncertainties [see Materials and Methods and (10)].

DISCUSSION

Our analysis of ship-tracks finds negligible global impact from the LWP adjustment, which supports the idea that the LWP adjustment is often overestimated, i.e., leading to excessively cooling effect, in current global climate models (GCMs) (10). However, it is quantitatively different from the strong warming effect reported in Toll *et al.* (10) that uses a similar approach. The discrepancy can be explained by the different data filters applied on their ship-track samples. We can reproduce their $d\ln LWP/d\ln N_d$ dependence on R_e if we apply the same filters, i.e., only keeping samples whose $\Delta R_e > 2 \text{ μm}$ and $\Delta N_d/N_d > 1$. However, such filters remove 72%

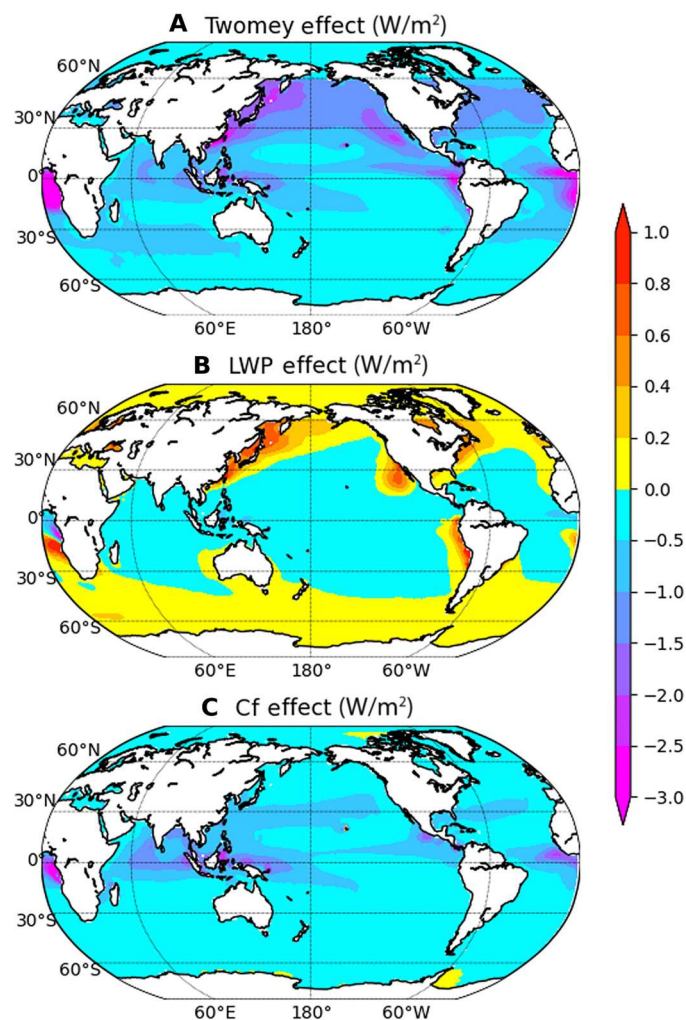


Fig. 6. Estimated forcings from different adjustments. The calculated aerosol indirect forcing contributions from the Twomey effect (A), the LWP adjustment (B), and the Cf adjustment (C).

of the samples and result in a notable shift of sampled background cloud properties toward those with higher R_e and LWP (see Materials and Methods and fig. S4), which drives the LWP adjustment to be more negative (fig. S5). ΔR_e and $\Delta N_d/N_d$ in ship-tracks depend on the background cloud conditions (37) and can have a wide range, with ΔR_e peaking between 0 and $1 \mu\text{m}$ (20, 38). Taken to the extreme, ship-emitted aerosols can affect clouds and radiation budget without detectable ship-tracks (23, 39). We believe that a less restrictive filter helps to obtain a more complete sampling of cloud conditions. Recent analysis indicates that LWP adjustment may produce strongly negative forcing in the so-called invisible ship-tracks (40).

The Cf adjustment is nonlinear and a function of multiple variables. We illustrate the sensitivity of the forcing from Cf adjustment to the choice of explanatory variables. Instead of a single explanatory variable, N_d , we calculate the dependence of the Cf adjustment as a function of two independent variables. The radiative forcing due to the Cf adjustment can be 212% of the Twomey effect, or -1.58 W m^{-2} , if we use N_d and background SST as explanatory

variables (see fig. S6 and table S2). The estimates from using different combinations of explanatory variables are summarized in table S2, and they range from 51% to 396% of the Twomey effect with a mean of 180% and a standard error of 53%. Because the multivariate approach should capture the nonlinearity more completely, our calculations suggest that the true effect of Cf adjustment may be underestimated using a single explanatory variable, which provides a lower bound (table S2).

The nonlinear dependence of dCf/dN_d on N_d implies that the effect of Cf adjustment is time-varying driven by the changing background N_d due to time-varying anthropogenic emissions. The Cf adjustment was the strongest when N_d was the lowest at preindustrial conditions (29, 41). It would be stronger than its present value in regions downwind of major anthropogenic pollution sources like Northern Pacific and Atlantic Oceans where N_d has substantially increased by human activity. As a consequence, the preindustrial level of N_d can meaningfully affect both the time evolution and absolute magnitude of radiative forcing due to the Cf adjustment. It is therefore important to accurately estimate the preindustrial N_d because uncertainties in preindustrial N_d can translate into large uncertainties in Cf adjustment induced forcing due to large dCf/dN_d at low N_d , similar to the sensitivity of the Twomey effect to preindustrial N_d (42). For example, the forcing due to the Cf adjustment can increase by 10% if we uniformly decrease the background N_d by just 5 cm^{-3} . Finally, when estimating ΔN_d between preindustrial and present day, it is important to consider the effects of aerosol speciation on N_d (43).

A few issues remain unaddressed in our study. We do not explicitly consider the time dependence of Cf and LWP adjustments to aerosols (24, 44, 45) because our analyses are based on instantaneous data although part of the time-dependent adjustments are implicitly included because our dataset includes ship-tracks of various ages (24). We follow previous studies (7, 10, 18) and extrapolate results from ship-tracks to the global ocean, which introduces uncertainty in our estimate of forcing. For example, LWP adjustment may introduce stronger cooling inside the trade cumulus regime than inside the stratocumulus regime that is the dominant regime sampled here (40). Extrapolating Cf effect derived mainly from the stratocumulus regime to the trade cumulus regime may introduce uncertainty because case studies using large-eddy simulations and observational analyses suggest that Cf can either decrease or increase in this regime (6, 15, 30). The potential choices of explanatory variables can also be expanded to include the underlying cloud morphology type and other cloud controlling factors. Several assumptions and approximations are also made in our calculations [see supplementary online materials (SOM)]. Our results are based on detectable ship-tracks, and we assume that given the same background clouds, they would have the same sensitivity to added aerosols and that sensitivity can be captured by detected ship-tracks. There are situations where clouds are affected by ship-emitted aerosols but do not produce detectable ship-tracks. It could be due to a combination of weak aerosol perturbation, already heavily polluted background clouds, unfavorable cloud types (25, 40), and/or unknown processes. Future studies are needed to comprehensively address these issues to further improve our understanding.

In summary, the magnitude of the radiative cooling effect of the Cf adjustment can be on par with the Twomey effect (16, 30, 46). Our results, based on an unprecedented number of ship-track

samples, suggest that it can range between 51 and 396% of the Twomey effect with a mean of 180%, which is in agreement with previous estimates with a range between 130 and 200% (7) using correlational analyses. GCMs also simulate Cf increase, primarily due to aerosols suppressing precipitation and increasing Cf (41). Process-level large-eddy simulations show a notable Cf increase under clean conditions for stratocumulus clouds (22, 23) while others show a slight decrease under different conditions, e.g., in the trade cumulus regime (6). Our analysis strongly supports a large cooling effect from the Cf adjustment under a variety of meteorological and cloud conditions that consistently show Cf increase with aerosols. The strong effect from Cf adjustment also points to clean and low Cf clouds as the most effective targets for climate intervention studies (47, 48). The observation-based relationships between the Cf sensitivity to aerosols and background N_d and R_e provide a quantitative constraint and benchmark to improve aerosol-cloud parameterizations in GCMs, which may help to reduce the uncertainty in aerosol indirect forcing and increase the confidence in climate projections of the future.

MATERIALS AND METHODS

As an overview, we derive LWP and Cf adjustments based on observations and analysis of ship-tracks. The key quantity to estimate is the ratio between forcings due to Cf and LWP adjustments and that of the Twomey effect with mostly observed variables. The ratio is fundamentally controlled by the sensitivity of Cf and LWP to N_d as shown by formulations discussed in detail in the following. While the absolute magnitudes of the Twomey effect and the Cf and LWP adjustments are sensitive to assumptions made and estimated ΔN_d as well as retrieval uncertainties, the ratio is much less susceptible (10). We have detailed discussions for the assumptions and potential sources of uncertainty in terms of the absolute magnitude in the following.

Analyzing cloud response in ship-tracks

For each detected ship-track, we automatically find background pixels in its surrounding. The width of these surrounding pixels is set to 20 pixels on both sides as shown in figs. S1 and S2. We do not include the one pixel just next to the edge of ship-track pixels to reduce the uncertainty around the edge and minimize the impact of potential aerosol-induced circulation changes in some ship-track cases that can create a positive Cf change bias (45). We then break each granule into blocks of size 128 pixels \times 128 pixels. Within each block, we calculate mean values of cloud variables such as droplet effective radius (R_e), cloud optical depth (COT), liquid water path (LWP), and cloud droplet number concentration (N_d) for the background and ship-track pixels. We consider the effect of cloud overlap when calculating Cf. We use the random overlap assumption: $Cf = (Cf_{\text{total}} - Cf_{\text{high}})/(1 - Cf_{\text{high}})$, where Cf, Cf_{total} , and Cf_{high} are low cloud fraction, total cloud fraction, and high cloud fraction, respectively. The Cf calculation is carried out separately for pixels within ship-track and surrounding masks as illustrated by examples in fig. S2. The difference between cloud properties inside background and ship-track masks is taken as the cloud response to ship-emitted aerosols. It is worth noting that our method allows for Cf adjustment in both positive and negative directions.

Pixels for which the cloud phase determined by infrared observations was identified as ice or mixed phase, and those with ice cloud retrievals are excluded. Only pixels with a single layer, according to MODIS cloud product multi-layer flag, and a low-level cloud (cloud top pressure > 650 hPa) were included. We also exclude the small ship-tracks that have less than 400 pixels because their size is too small to obtain accurate cloud fraction. The track segments were included in the analyses only when the R_e difference between ship-track and background clouds was less than $-0.5 \mu\text{m}$ and the relative changes of N_d was larger than 20%. We choose to filter the data this way because of small uncertainty range of R_e retrievals and larger uncertainty in N_d . For R_e , the relative uncertainty for liquid clouds ranges between 1.5 and around 10% (17) while it is 78% for N_d at the pixel level. Because each ship-track sample typically contains hundreds of pixels and ensemble mean can reduce the magnitude of uncertainty, we select the threshold to be $0.5 \mu\text{m}$ and 20% for R_e and N_d , respectively. This choice has minimal impact on the probability distributions of cloud properties when comparing the filtered clouds and all samples (e.g., fig. S4). Further decreasing of their thresholds makes the calculation of the adjustments, which are derivatives, prone to uncertainties in these two variables. In total, there are 295,036 such ship-track blocks that satisfy our conditions. If we follow the criteria $\Delta R_e > 2.0 \mu\text{m}$ used in Toll *et al.* (10), the number of samples decreases to 164,626. If the additional condition of $\Delta N_d/N_d > 1$ is applied (10), the number of samples decreases to 83,155, representing a more than 72% decrease. It is also worth noting that here that we do not use any proxy such as aerosol optical depth or aerosol index for N_d because we can confidently attribute the changes of N_d between ship-track and background clouds to aerosols.

We group blocks based on their background N_d , or other variables of choice, into a number of bins. For each bin, we calculate mean cloud responses and their 95% uncertainty ranges based on samples that fall within this bin. The dependence of cloud responses to background cloud variables can thus be obtained using this approach. The approach can be extended to two-dimensional (2D) bins based on two explanatory variables, e.g., N_d and Cf, and we can obtain a 2D cloud response function. Once the relationships and their uncertainty ranges are derived, we assume that similar relationships apply in regions that do not have high numbers of ship-track samples; i.e., we assume the same physics apply (10).

Calculating aerosol indirect forcing

Without considering aerosol effects on cloud fractions, cloud albedo sensitivity to aerosols can be taken as the sum of the Twomey effect and aerosol-induced LWP adjustments (10):

$$S = \frac{dA_c}{dN_d} = \frac{A_c(1 - A_c)}{3N_d} \times \left(1 + \frac{5 \ln LWP}{2 \ln N_d} \right) \quad (1)$$

where S is the susceptibility of cloud albedo (A_c) to droplet number concentration N_d (10).

If we only consider the Twomey effect and LWP adjustment, we have

$$\Delta SW_{\text{TOA}} = -SW_{\text{downwelling}} \times Cf \times S \times \Delta N_d \quad (2)$$

Aerosol indirect forcing is therefore

$$\Delta SW_{\text{TOA}} = -SW_{\text{downwelling}} \times Cf \times A_c \times (1 - A_c) \times \left(\frac{1}{3} + \frac{5}{6} \frac{d \ln LWP}{d \ln N_d} \right) \times \Delta \ln N_d \quad (3)$$

$SW_{\text{downwelling}}$ is shortwave flux at the clouds. It can be conservatively estimated using the Clouds and the Earth's Radiant Energy System (CERES) clear sky surface downwelling shortwave flux. Cf is low cloud fraction. We use the MODIS L3 product to derive it. A_c is the cloud albedo; it can be calculated from the CERES all-sky albedo (A_{allsky}), clear-sky albedo (A_{clearsky}), and total cloud fraction (Cf_{total}) using the equation

$$A_c = (A_{\text{allsky}} - (1 - Cf_{\text{total}}) \times A_{\text{clearsky}}) / Cf_{\text{total}} \quad (4)$$

The CERES and MODIS data we used are 2003 to 2020 monthly mean $1^\circ \times 1^\circ$ global data of the CERES Energy Balance and Filled Top of the Atmosphere (EBAF-TOA) (49) and the MYD08_M3 (50) products, respectively. We calculated the 2003 to 2020 climatological-mean $SW_{\text{downwelling}}$, Cf , and A_c , and interpolated them to $2^\circ \times 2^\circ$ horizontal resolution.

From the analysis of cloud response in ship-tracks, we first calculated the relative differences in LWP ($d \ln LWP$) and the relative differences in N_d ($d \ln N_d$) between ship-track blocks and their control counterparts, and thereby derived their ratios $\frac{d \ln LWP}{d \ln N_d}$ for all ship-track samples. We then sorted these $\frac{d \ln LWP}{d \ln N_d}$ by their control cloud N_d , and calculated mean values of $\frac{d \ln LWP}{d \ln N_d}$ for each control N_d bin. The dependence of $\frac{d \ln LWP}{d \ln N_d}$ on N_d is used as our function to calculate the LWP adjustment. For global $2^\circ \times 2^\circ$ grids, we first calculated 2003 to 2020 climatological-mean N_d from the MYD08_M3 data. On the basis of the 1D dependence of $\frac{d \ln LWP}{d \ln N_d}$ on N_d , we derive the global gridded LWP adjustment sensitivity, $\frac{d \ln LWP}{d \ln N_d}$. $\Delta \ln N_d$ and ΔN_d are calculated in the same way as Toll *et al.* (10). It is based on the model-simulated aerosol optical depth (AOD) difference between preindustrial and present and empirical relationship between AOD and N_d . To make our results and those from Toll *et al.* comparable, we adopt the same method. For details, please refer to their paper. With all these variables ready, we calculate the global gridded values of aerosol indirect forcing due to the LWP adjustment to N_d .

To consider the effect of Cf adjustment due to aerosols, we consider the sensitivity of scene albedo (A) to N_d . $A = A_{ac} Cf_{\text{total}} + A_s(1 - Cf_{\text{total}})$ (51). We have

$$S^* = \frac{dA}{dN_d} = \frac{d[A_{ac} Cf_{\text{total}} + A_s(1 - Cf_{\text{total}})]}{dN_d} \approx Cf \times S + (1 - Cf_{\text{high}}) \times \frac{dCf}{dN_d} \times (A_{ac} - A_s) \quad (5)$$

where A is the scene albedo, i.e., including both cloudy, A_{ac} , and clear, A_s , parts; Cf_{total} and Cf are all cloud and low cloud fraction obtained from the MYD08_M3 data; A_s is the surface albedo, derived from the CERES EBAF-TOA data (49); $1 - Cf_{\text{high}}$ is used to take into account the effect of overlap on Cf adjustment. We assume minimum aerosol effects on high clouds. $\frac{dCf}{dN_d}$ is calculated using our ship-track samples, similar to the LWP adjustment. We account for the cloud overlap between high and low clouds when calculating Cf for both background and ship-track clouds to

reflect its true values. Here, we use the random overlap assumption, but tests with other overlap assumptions show minimum impact. We first calculate $\frac{dCf}{dN_d}$ for each ship-track sample and sort them by their corresponding control cloud N_d . We then average values of $\frac{dCf}{dN_d}$ for each control N_d bin and obtain the 1D dependence of $\frac{dCf}{dN_d}$ on N_d . On lat-lon grid, $\frac{dCf}{dN_d}$ is obtained based on its N_d according to the $\frac{dCf}{dN_d}$ versus N_d relationship, similar to the LWP adjustment (10). In addition, we calculate $\frac{dCf}{dN_d}$ and average them as a function of a pair of explanatory variables such as N_d - Cf , N_d -EIS, and N_d -SST. We then obtain the 2D dependence of $\frac{dCf}{dN_d}$ on N_d and Cf , or other paired variables. Using this 2D dependence of $\frac{dCf}{dN_d}$, we derive global gridded $\frac{dCf}{dN_d}$, and calculate S^* and changes of TOA SW flux due to cloud coverage effect using the equation

$$\Delta SW_{\text{TOA}} = -SW_{\text{downwelling}} \times S^* \times \Delta N_d \quad (6)$$

To study the influences of meteorological conditions on the Cf adjustments to aerosols, we collocate the Modern-Era Retrospective analysis for Research and Applications (MERRA2) 2D hourly (inst1_2d_asm_Nx) data and 3D 3-hourly (inst3_3d_asm_Np) reanalysis data (52) with our ship-track and control clouds. We calculate mean values of the collocated MERRA2 RH, SST, and EIS for every ship-track block and background clouds. The Cf adjustments of individual ship-track sample are averaged based on the explanatory variable or pair of explanatory variables such as control cloud N_d , N_d and SST, and N_d and EIS. We thus obtain the 2D dependence of $\frac{dCf}{dN_d}$ on N_d and Cf , N_d and SST, and N_d and EIS, respectively. Using these 2D $\frac{dCf}{dN_d}$ dependences as the lookup table, we derived global gridded $\frac{dCf}{dN_d}$, and then calculated S^* and cloud coverage effects on the TOA SW flux. We also tried to derive 3D dependence of $\frac{dCf}{dN_d}$ on N_d , EIS, and RH, and N_d , Cf , and RH. Similarly, we calculate the $\frac{d \ln LWP}{d \ln N_d}$ and its dependence on background RH, EIS, and SST using the MERRA-2 data.

We propagate the uncertainties of our estimates of $\frac{dCf}{dN_d}$ and $\frac{d \ln LWP}{d \ln N_d}$ and their dependence on N_d to uncertainty in forcing estimates. For each N_d , we find the 95 or 99% confidence intervals for the mean values of $\frac{dCf}{dN_d}$ and $\frac{d \ln LWP}{d \ln N_d}$. We then apply the upper and lower limits of the Cf and LWP sensitivity to each grid point and obtain the upper and lower bound for indirect forcing due to Cf and LWP adjustments. The results are presented in table S1. The forcing due to the LWP adjustment has a relatively larger range than that of the Cf adjustment.

The total forcing calculated using different sets of explanatory variables including N_d and Cf , N_d and SST, and N_d and EIS is presented in table S2. For reference, we also include the number when using only N_d . Adding above cloud RH does not appreciably change the forcing, which agrees with our finding that the Cf adjustment is not sensitive to above cloud RH. The largest forcing is obtained with the N_d and Cf combination and it represents more than 396% of the Twomey effect. The ratios are 212% and 75% when using N_d and SST, and N_d and EIS, respectively. We also test with using three explanatory variables. The ratios are 384 and 97% when N_d , Cf , and RH, and N_d , EIS, and RH are used, respectively. In all, the range

spans between 51 and 396% and the mean of ratios is 180% with a standard error of 53%.

We note a few assumptions and approximations adopted in our method of estimating the absolute aerosol indirect forcing detailed above. It is worth noting again that the ratio between effects of LWP and Cf adjustments and the Twomey effect is less susceptible to such assumptions. For example, the change in N_d can be substantial such that the condition $d\ln N_d \ll 1$ is not satisfied and an integration is required to more accurately calculate the forcing. Similarly, an integration should be applied to the LWP and Cf adjustment calculations. We adopted the approximation because we do not know the exact functional form of the LWP and Cf adjustments and we want to compare the relative importance of the Twomey and the adjustment effects (7, 10). We used $SW_{\text{downwelling}}$ at the surface from CERES in Eq. 2 instead of $SW_{\text{downwelling}}$ at the cloud top, which underestimates the total forcing because $SW_{\text{downwelling}}$ at the cloud top is larger. At the same time, we do not account for the transmittance from cloud top to the top of the atmosphere, which overestimates the forcing. This assumption is made because of the lack of observations for these quantities; finally, the LWP and Cf adjustments can be sensitive to more variables that are considered here. We adopted such approximations and assumptions due to the limit of observables (e.g., the $SW_{\text{downwelling}}$) and amount of available data (e.g., sensitivity of $\frac{dCf}{dN_d}$ and $\frac{d\ln LWP}{d\ln N_d}$ to multiple variables). Also, we assume that the derived $\frac{dCf}{dN_d}$ and $\frac{d\ln LWP}{d\ln N_d}$ and their dependence on background variables apply to regions that have less ship-track samples. Here, our goal is to provide a first estimate of the ratio based on best available observations and practices in the literature while being aware of such assumptions and approximations (7, 10). Also, potential semi-direct effects due to absorbing aerosols from ship emissions are not explicitly addressed in this study because we do not have enough observational information to separate it out.

Supplementary Materials

This PDF file includes:

Tables S1 and S2

Figs. S1 to S7

REFERENCES AND NOTES

1. S. Twomey, The influence of pollution on the shortwave albedo of clouds. *J. Atmos. Sci.* **34**, 1149–1152 (1977).
2. B. Albrecht, Aerosols, cloud microphysics, and fractional cloudiness. *Science* **245**, 1227–1230 (1989).
3. P. Forster, T. Storelvmo, K. Armour, W. Collins, J.-L. Dufresne, D. Frame, D. J. Lunt, T. Mauritsen, M. D. Palmer, M. Watanabe, M. Wild, H. Zhang, The Earth's energy budget, climate feedbacks, and climate sensitivity, in *Climate Change 2021: The Physical Science Basis. Contribution of Working Group I to the Sixth Assessment Report of the Intergovernmental Panel on Climate Change* (Cambridge Univ. Press, 2021).
4. D. Victor, D. Zhou, E. H. M. Ahmed, P. K. Dadhich, J. Olivier, H.-H. Rogner, K. Sheikh, M. Yamaguchi, Introductory chapter, in *AR5 Climate Change 2014: Mitigation of Climate Change from Working Group III* (Cambridge Univ. Press, 2014).
5. A. S. Ackerman, M. P. Kirkpatrick, D. E. Stevens, O. B. Toon, The impact of humidity above stratiform clouds on indirect aerosol climate forcing. *Nature* **432**, 1014–1017 (2004).
6. B. Stevens, G. Feingold, Untangling aerosol effects on clouds and precipitation in a buffered system. *Nature* **461**, 607–613 (2009).
7. N. Bellouin, J. Quaas, E. Gryspeerdt, S. Kinne, P. Stier, D. Watson-Parris, O. Boucher, K. S. Carslaw, M. Christensen, A.-L. Daniau, J.-L. Dufresne, G. Feingold, S. Fiedler, P. Forster, A. Gettelman, J. M. Haywood, U. Lohmann, F. Malavelle, T. Mauritsen, D. T. McCoy, G. Myhre, J. Mülmenstädt, D. Neubauer, A. Possner, M. Rugenstein, Y. Sato, M. Schulz, S. E. Schwartz, O. Sourdeval, T. Storelvmo, V. Toll, D. Winker, B. Stevens, Bounding global aerosol radiative forcing of climate change. *Rev. Geophys.* **58**, e2019RG000660 (2020).
8. Y.-C. Chen, M. W. Christensen, G. L. Stephens, J. H. Seinfeld, Satellite-based estimate of global aerosol–cloud radiative forcing by marine warm clouds. *Nat. Geosci.* **7**, 643–646 (2014).
9. M. D. Lebsock, G. L. Stephens, C. Kummerow, Multisensor satellite observations of aerosol effects on warm clouds. *J. Geophys. Res. Atmos.* **113**, D15205 (2008).
10. V. Toll, M. Christensen, J. Quaas, N. Bellouin, Weak average liquid-cloud-water response to anthropogenic aerosols. *Nature* **572**, 51–55 (2019).
11. D. Rosenfeld, Y. J. Kaufman, I. Koren, Switching cloud cover and dynamical regimes from open to closed Benard cells in response to the suppression of precipitation by aerosols. *Atmospheric Chem. Phys.* **6**, 2503–2511 (2006).
12. T. Goren, D. Rosenfeld, Satellite observations of ship emission induced transitions from broken to closed cell marine stratocumulus over large areas. *J. Geophys. Res. Atmos.* **117**, D17206 (2012).
13. Y. Wang, X. Zheng, X. Dong, B. Xi, P. Wu, T. Logan, Y. L. Yung, Impacts of long-range transport of aerosols on marine-boundary-layer clouds in the eastern North Atlantic. *Atmos. Chem. Phys.* **20**, 14741–14755 (2020).
14. M. W. Christensen, W. K. Jones, P. Stier, Aerosols enhance cloud lifetime and brightness along the stratus-to-cumulus transition. *Proc. Natl. Acad. Sci. U.S.A.* **117**, 17591–17598 (2020).
15. D. Rosenfeld, Y. Zhu, M. Wang, Y. Zheng, T. Goren, S. Yu, Aerosol-driven droplet concentrations dominate coverage and water of oceanic low-level clouds. *Science* **363**, eaav0566 (2019).
16. E. Gryspeerdt, J. Quaas, N. Bellouin, Constraining the aerosol influence on cloud fraction. *J. Geophys. Res. Atmos.* **121**, 3566–3583 (2016).
17. D. P. Grosvenor, O. Sourdeval, P. Zuidema, A. Ackerman, M. D. Alexandrov, R. Bennartz, R. Boers, B. Cairns, J. C. Chiu, M. Christensen, H. Deneke, M. Diamond, G. Feingold, A. Fridlind, A. Hünerbein, C. Knist, P. Kollias, A. Marshak, D. McCoy, D. Merk, D. Painemal, J. Rausch, D. Rosenfeld, H. Russchenberg, P. Seifert, K. Sinclair, P. Stier, B. van Diedenhoven, M. Wendisch, F. Werner, R. Wood, Z. Zhang, J. Quaas, Remote sensing of droplet number concentration in warm clouds: A review of the current state of knowledge and perspectives. *Rev. Geophys.* **56**, 409–453 (2018).
18. M. W. Christensen, A. Gettelman, J. Cermak, G. Dagan, M. Diamond, A. Douglas, G. Feingold, F. Glassmeier, T. Goren, D. P. Grosvenor, E. Gryspeerdt, R. Kahn, Z. Li, P.-L. Ma, F. Malavelle, I. L. McCoy, D. T. McCoy, G. McFarquhar, J. Mülmenstädt, S. Pal, A. Possner, A. Povey, J. Quaas, D. Rosenfeld, A. Schmidt, R. Schrödner, A. Sorooshian, P. Stier, V. Toll, D. Watson-Parris, R. Wood, M. Yang, T. Yuan, Opportunistic experiments to constrain aerosol effective radiative forcing. *Atmos. Chem. Phys.* **22**, 641–674 (2022).
19. Y.-C. Chen, M. W. Christensen, L. Xue, A. Sorooshian, G. L. Stephens, R. M. Rasmussen, J. H. Seinfeld, Occurrence of lower cloud albedo in ship tracks. *Atmos. Chem. Phys.* **12**, 8223–8235 (2012).
20. M. W. Christensen, G. L. Stephens, Microphysical and macrophysical responses of marine stratocumulus polluted by underlying ships: Evidence of cloud deepening. *J. Geophys. Res.* **116**, D03201 (2011).
21. S. Hu, Y. Zhu, D. Rosenfeld, F. Mao, X. Lu, Z. Pan, L. Zang, W. Gong, The dependence of ship-polluted marine cloud properties and radiative forcing on background drop concentrations. *J. Geophys. Res. Atmos.* **126**, e2020JD033852 (2021).
22. H. Wang, P. J. Rasch, G. Feingold, Manipulating marine stratocumulus cloud amount and albedo: A process-modelling study of aerosol–cloud–precipitation interactions in response to injection of cloud condensation nuclei. *Atmos. Chem. Phys.* **11**, 4237–4249 (2011).
23. A. Possner, H. Wang, R. Wood, K. Caldeira, T. P. Ackerman, The efficacy of aerosol–cloud radiative perturbations from near-surface emissions in deep open-cell stratocumuli. *Atmos. Chem. Phys.* **18**, 17475–17488 (2018).
24. E. Gryspeerdt, T. Goren, T. W. P. Smith, Observing the timescales of aerosol–cloud interactions in snapshot satellite images. *Atmos. Chem. Phys.* **21**, 6093–6109 (2020).
25. T. Yuan, H. Song, C. Wang, L. Oreopoulos, S. E. Platnick, S. von Hippel, K. G. Meyer, S. Light, E. Wilcox, Global reduction in ship-tracks from sulfur regulations for shipping fuel. *Sci. Adv.* **8**, eabn7988 (2022).
26. T. Yuan, C. Wang, H. Song, S. Platnick, K. Meyer, L. Oreopoulos, Automatically finding ship tracks to enable large-scale analysis of aerosol–cloud interactions. *Geophys. Res. Lett.* **46**, 7726–7733 (2019).
27. R. Wood, C. S. Bretherton, On the relationship between stratiform low cloud cover and lower-tropospheric stability. *J. Climate* **19**, 6425–6432 (2006).
28. D. Rosenfeld, H. Wang, P. J. Rasch, The roles of cloud drop effective radius and LW Pin determining rain properties in marine stratocumulus. *Geophys. Res. Lett.* **39**, L13801 (2012).
29. I. Koren, G. Dagan, O. Altartaz, From aerosol-limited to invigoration of warm convective clouds. *Science* 10.1126/science.1252595, 344, 1143–1146 (2014).

30. T. Yuan, L. A. Remer, H. Yu, Microphysical, macrophysical and radiative signatures of volcanic aerosols in trade wind cumulus observed by the A-train. *Atmos. Chem. Phys.* **11**, 7119–7132 (2011).
31. R. Wood, D. L. Hartmann, Spatial variability of liquid water path in marine low cloud: The importance of mesoscale cellular convection. *J. Climate* **19**, 1748–1764 (2006).
32. A. Muehlbauer, I. L. McCoy, R. Wood, Climatology of stratocumulus cloud morphologies: Microphysical properties and radiative effects. *Atmos. Chem. Phys.* **14**, 6695–6716 (2014).
33. F. F. Malavelle, J. M. Haywood, A. Jones, A. Gettelman, L. Clarisse, S. Bauduin, R. P. Allan, I. H. H. Karset, J. E. Kristjánsson, L. Oreopoulos, N. Cho, D. Lee, N. Bellouin, O. Boucher, D. P. Grosvenor, K. S. Carslaw, S. Dhomse, G. W. Mann, A. Schmidt, H. Coe, M. E. Hartley, M. Dalvi, A. A. Hill, B. T. Johnson, C. E. Johnson, J. R. Knight, F. M. O'Connor, D. G. Partridge, P. Stier, G. Myhre, S. Platnick, G. L. Stephens, H. Takahashi, T. Thordarson, Strong constraints on aerosol–cloud interactions from volcanic eruptions. *Nature* **546**, 485–491 (2017).
34. C. R. Terai, M. S. Pritchard, P. Blossy, C. S. Bretherton, The impact of resolving subkilometer processes on aerosol–cloud interactions of low-level clouds in global model simulations. *J. Adv. Model. Earth Syst.* **12**, e2020MS002274 (2020).
35. A. Slingo, Sensitivity of the Earth's radiation budget to changes in low clouds. *Nature* **343**, 49–51 (1990).
36. D. A. Randall, J. A. Coakley Jr., C. W. Fairall, R. A. Kropfli, D. H. Lenschow, Outlook for research on subtropical marine stratification clouds. *Bull. Am. Meteorol. Soc.* **65**, 1290–1301 (1984).
37. S. Platnick, P. A. Durkee, K. Nielsen, J. P. Taylor, S. C. Tsay, M. D. King, R. J. Ferek, P. V. Hobbs, J. W. Rottman, The role of background cloud microphysics in the radiative formation of ship tracks. *J. Atmos. Sci.* **57**, 2607–2624 (2000).
38. P. A. Durkee, K. J. Noone, R. J. Ferek, D. W. Johnson, J. P. Taylor, T. J. Garrett, P. V. Hobbs, J. G. Hudson, C. S. Bretherton, G. Innis, G. M. Frick, W. A. Hoppel, C. D. O'Dowd, L. M. Russell, R. Gasparovic, K. E. Nielsen, S. A. Tessmer, E. Öström, S. R. Osborne, R. C. Flagan, J. H. Seinfeld, H. Rand, The impact of ship-produced aerosols on the microstructure and albedo of warm marine stratocumulus clouds: A test of MAST hypotheses Ii and Iii. *J. Atmos. Sci.* **57**, 2554–2569 (2000).
39. M. S. Diamond, H. M. Director, R. Eastman, A. Possner, R. Wood, Using observations to better understand aerosol–cloudclimate interactions. *AGU Adv.* **1**, e2019AV000111 (2020).
40. P. Manshausen, D. Watson-Parris, M. W. Christensen, J.-P. Jalkanen, P. Stier, Invisible ship tracks show large cloud sensitivity to aerosol. *Nature* **610**, 101–106 (2022).
41. S. Ghan, M. Wang, S. Zhang, S. Ferrachat, A. Gettelman, J. Griesfeller, Z. Kipling, U. Lohmann, H. Morrison, D. Neubauer, D. G. Partridge, P. Stier, T. Takemura, H. Wang, K. Zhang, Challenges in constraining anthropogenic aerosol effects on cloud radiative forcing using present-day spatiotemporal variability. *Proc. Natl. Acad. Sci. U.S.A.* **113**, 5804–5811 (2016).
42. K. S. Carslaw, L. A. Lee, C. L. Reddington, K. J. Pringle, A. Rap, P. M. Forster, G. W. Mann, D. V. Spracklen, M. T. Woodhouse, L. A. Regayre, J. R. Pierce, Large contribution of natural aerosols to uncertainty in indirect forcing. *Nature* **503**, 67–71 (2013).
43. P. V. Hobbs, T. J. Garrett, R. J. Ferek, S. R. Strader, D. A. Hegg, G. M. Frick, W. A. Hoppel, R. F. Gasparovic, L. M. Russell, D. W. Johnson, C. O'Dowd, P. A. Durkee, K. E. Nielsen, G. Innis, Emissions from ships with respect to their effects on clouds. *J. Atmos. Sci.* **57**, 2570–2590 (2000).
44. F. Glasmeier, F. Hoffmann, J. S. Johnson, T. Yamaguchi, K. S. Carslaw, G. Feingold, Aerosol–cloud–climate cooling overestimated by ship-track data. *Science* **371**, 485–489 (2021).
45. H. Wang, G. Feingold, Modeling mesoscale cellular structures and drizzle in marine stratocumulus. Part II: The microphysics and dynamics of the boundary region between open and closed cells. *J. Atmos. Sci.* **66**, 3257–3275 (2009).
46. M. W. Christensen, D. Neubauer, C. A. Poulsen, G. E. Thomas, G. R. McGarragh, A. C. Povey, S. R. Proud, R. G. Grainger, Unveiling aerosol–cloud interactions—Part 1: Cloud contamination in satellite products enhances the aerosol indirect forcing estimate. *Atmos. Chem. Phys.* **17**, 13151–13164 (2017).
47. R. Wood, Assessing the potential efficacy of marine cloud brightening for cooling Earth using a simple heuristic model. *Atmospheric Chem. Phys. Discuss.*, 1–52 (2021).
48. Y. Chen, J. Haywood, Y. Wang, F. Malavelle, G. Jordan, D. Partridge, J. Fieldsend, J. De Leeuw, A. Schmidt, N. Cho, L. Oreopoulos, S. Platnick, D. Grosvenor, P. Field, U. Lohmann, Machine learning reveals climate forcing from aerosols is dominated by increased cloud cover. *Nat. Geosci.* **15**, 609–614 (2022).
49. N. G. Loeb, D. R. Doelling, H. Wang, W. Su, C. Nguyen, J. G. Corbett, L. Liang, C. Mitrescu, F. G. Rose, S. Kato, Clouds and the Earth's Radiant Energy System (CERES) Energy Balanced and Filled (EBAF) Top-of-Atmosphere (TOA) edition-4.0 data product. *J. Clim.* **31**, 895–918 (2018).
50. S. Platnick, K. G. Meyer, M. D. King, G. Wind, N. Amarasinghe, B. Marchant, G. T. Arnold, Z. Zhang, P. A. Hubanks, R. E. Holz, P. Yang, W. L. Ridgway, J. Riedi, The MODIS cloud optical and microphysical products: Collection 6 updates and examples from terra and aqua. *IEEE Trans. Geosci. Remote Sens.* **55**, 502–525 (2017).
51. M. Webb, C. Senior, S. Bony, J.-J. Morcrette, Combining ERBE and ISCCP data to assess clouds in the Hadley Centre, ECMWF and LMD atmospheric climate models. *Clim. Dynam.* **17**, 905–922 (2001).
52. R. Gelaro, W. McCarty, M. J. Suárez, R. Todling, A. Molod, L. Takacs, C. A. Randles, A. Darmenov, M. G. Bosilovich, R. Reichle, K. Wargan, L. Coy, R. Cullather, C. Draper, S. Akella, V. Buchard, A. Conaty, A. M. da Silva, W. Gu, G.-K. Kim, R. Koster, R. Lucchesi, D. Merkova, J. E. Nielsen, G. Partyka, S. Pawson, W. Putman, M. Rienecker, S. D. Schubert, M. Sienkiewicz, B. Zhao, The modern-era retrospective analysis for research and applications, Version 2 (MERRA-2). *J. Climate* **30**, 5419–5454 (2017).

Acknowledgments: We thank an anonymous reviewer and the editor for helpful comments and suggestions that improved the paper's quality. **Funding:** This work was supported by the National Aeronautics and Space Administration (grant numbers: 80NSSC18M0084 and NNH20ZDA001N-TASNP). **Author contributions:** T.Y. conceived the idea, designed the experiments, and wrote the draft. All authors contributed to the writing of the manuscript and discussion of the results. H.S. conducted the data processing. **Competing interests:** The authors declare that they have no competing interests. **Data and materials availability:** The MODIS cloud product, CERES flux and albedo product, and the MERRA2 data used in this study are available from the Atmosphere Archive and Distribution System (LAADS) Distributed Active Archive Center (DAAC) (<https://ladsweb.nascom.nasa.gov/>), CERES (<https://ceres.larc.nasa.gov/data/>), and the Global Modeling and Assimilation Office (https://gmao.gsfc.nasa.gov/reanalysis/MERRA-2/data_access/). The ship-track blocks data are available at <https://doi.org/10.7910/DVN/JII4DN>. All data needed to evaluate the conclusions in the paper are present in the paper and/or the Supplementary Materials.

Submitted 14 March 2023
 Accepted 4 October 2023
 Published 8 November 2023
 10.1126/sciadv.adh7716

Observational evidence of strong forcing from aerosol effect on low cloud coverage

Tianle Yuan, Hua Song, Robert Wood, Lazaros Oreopoulos, Steven Platnick, Chenxi Wang, Hongbin Yu, Kerry Meyer, and Eric Wilcox

Sci. Adv. **9** (45), eadh7716. DOI: 10.1126/sciadv.adh7716

View the article online

<https://www.science.org/doi/10.1126/sciadv.adh7716>

Permissions

<https://www.science.org/help/reprints-and-permissions>

Use of this article is subject to the [Terms of service](#)

Science Advances (ISSN 2375-2548) is published by the American Association for the Advancement of Science. 1200 New York Avenue NW, Washington, DC 20005. The title *Science Advances* is a registered trademark of AAAS.

Copyright © 2023 The Authors, some rights reserved; exclusive licensee American Association for the Advancement of Science. No claim to original U.S. Government Works. Distributed under a Creative Commons Attribution NonCommercial License 4.0 (CC BY-NC).